Supporting Information File

Mechanochromic Hydrogen-Bonded Cocrystals with Salient Effect Upon Heating

Armando Navarro-Huerta[a], Antonio Juárez-Calixto,[a] María Eugenia Sandoval-Salinas[b], Yoarhy A. Amador-Sánchez[c], Joelis Rodríguez-Hernández[d], Alejandra Núñez-Pineda[a,e], Mario Rodríguez[f], Rachel Crespo-Otero[b] and Braulio Rodríguez-Molina[a,*]

[a]*Instituto de Química, Universidad Nacional Autónoma de México, Circuito Exterior S/N Ciudad Universitaria, Coyoacán 04510, Mexico City, Mexico.*

[b]*UCL Department of Chemistry, London WC1H 0AJ, United Kingdom.*

[c]*Laboratorio de Fisicoquímica y Reactividad de Superficies (LaFReS), Instituto de Investigaciones en Materiales, Universidad Nacional Autónoma de México, Circuito Exterior S/N Ciudad Universitaria, Coyoacán 04510, Mexico City, Mexico.*

[d]*Centro de Investigación en Química Aplicada (CIQA), Boulevard Enrique Reyna Hermosillo No. 140, Saltillo 25294, Coahuila, Mexico.*

[e]*Centro Conjunto de Investigación en Química Sustentable (CCIQS) UAEM-UNAM, Carretera Toluca-Atlacomulco Km. 14.5, Toluca, Estado de México, Mexico.*

[f]*Research Group of Optical Properties of Materials (GPOM), Centro de Investigaciones en Óptica, CIO, Apdo. Postal 1-948, León 37000, Guanajuato, México.*

*brodriguez@iquimica.unam.mx

Materials and methods

Reagents and solvents were purchased from company Sigma-Aldrich®. Reactions were monitored through TLC using silica gel plates 60 F_{254} purchased from Merck®. Spots were detected by UV-light absorption. Reactions were carried out in inert atmosphere using nitrogen (N_2). Solution ^{1}H and ^{13}C experiments were recorded at room temperature using a Jeol Eclipse 300. The spectroscopic data is referenced to $CDCl_3$ (^{1}H: δ = 7.26 ppm, s; ^{13}C: δ = 77.0 ppm). High-Resolution Mass Spectrometry was obtained in a Jeol JMS-AccuTOF JMS-T100LC spectrometer, ionization mode: Direct Analysis in Real Time (DART). FTIR spectra experiments were recorded with Bruker ATR equipped with a diamond tip in the spectral window from 4000 to 500 cm^{-1}. Uncorrected melting points were determined in a Fisher-Johns melting point apparatus, unless otherwise noted.

Synthesis of 9-(*N*-carbazolyl)acridine (AC)

Synthesis of AC has been previously reported by Zeghada et. al. in 2020.[S1] The procedure was replicated as stated there. Quantities: 180 mg (1.0 mmol, 1.0 eq.) of acridine, 168 mg (1.0 mmol, 1.0 eq) of carbazole, 654.5 mg (2.01 mmol, 2.0 eq.) of Cs_2CO_3, 38 mg (0.2 mmol, 0.2 eq.) of CuI and 0.5 mL of dry DMSO. The mixture was heated to 110 °C for 24 hours under nitrogen atmosphere.

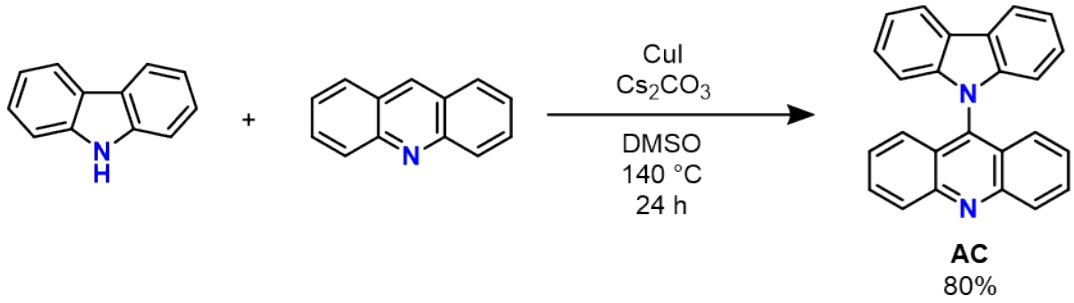

Scheme S1. Synthetic route for the obtaining of AC molecule.

The purification of the compound was carried out by pouring water into the reaction mixture and filtering the solids in vacuum. Then, the solids were redissolved in ethyl acetate, dried with Na_2SO_4 and filtered through cotton. The mixture was then supported in silica gel and purified by column chromatography, using a gradient eluent (hexanes → hexanes/ethyl acetate 85:15) to obtain a pure yellow powder (276 mg, 80% yield). Melting point: 255 °C (as solvent free form, determined by coupled DSC/TGA). **^{1}H NMR** (300 MHz, $CDCl_3$, Room temperature) δ: 8.42 (d, *J* = 8.8 Hz, 2H), 8.29 (d, *J* = 7.7 Hz, 2H), 7.86 – 7.80 (m, 2H), 7.39 – 7.28 (m, 8H), 6.76 (d, *J* = 7.6 Hz, 2H). **^{13}C NMR** (75 MHz, $CDCl_3$, Room temperature) δ:150.2, 142.3, 139.7, 130.9, 130.2, 127.2, 126.5, 124.6, 124.0, 123.6, 120.7, 120.7, 110.4. **FTIR** (ATR, cm^{-1}) ν: 3036, 2922, 2851, 1620, 1593, 1554, 1517, 1475, 1447, 1419, 1312, 1227, 1147, 1012, 920, 857, 743, 721, 630, 607. **HRMS** (DART) m/z: $[C_{25}H_{17}N_2]^+$, calculated 345.13917, found 345.13864, difference (ppm): -1.54. To obtain the single crystals, the

compound can be recrystallized from acetonitrile (solvent free), THF/methanol (THF solvate) or toluene (Toluene solvate). In all cases, yellow prismatic crystals are obtained.

Hirshfeld fingerplots and energy frameworks in cocrystals

Hirshfeld surface calculations and interaction energies were calculated using *CrystalExplorer 21.5*®,[S2] using the *CE*-B3LYP 6-31G(d,p) functional integrated in the software. Isosurfaces are displayed at 0.002 a.u. The scale factors for electrostatic, dispersion, polarization and repulsion are depicted in the table below. SC XRD structures of **AC-TFTA** and **AC-PFBA** were employed for the calculations.

Scale factors for functional used in Hirshfeld surfaces calculations.

CE-B3LYP/6-31G(d,p)	k_{elec}	k_{disp}	k_{pol}	k_{rep}
	1.057	0.740	0.871	0.618

Computational details

The crystalline structures of AC, TFTA and PFBA crystals and AC-TFTA and AC-PFBA co-crystals were refined to optimize the Hydrogen and Oxygen positions by using Periodic Density Functional Theory with PBE and dispersion correction (D2 scheme)[S3] with the Vienna Ab Initio Simulation Package (VASP) version 5.4.4.[S4]

The photophysical properties of AC crystal and AC-PFBA and AC-TFTA co-crystals were modeled within the ONIOM(QM:QM') embedded cluster model as implemented in the fromage code.[S5,S6] Semi spherical clusters with radius ~20 Å were used, where the QM region includes a monomer (AC), dimer (AC-PFBA) and trimer (AC-TFTA) and treated at the CAM-B3LYP/6-311++G(d,p) level of theory[7] including Grimme's dispersion correction (D3)[8] with the program package Gaussian16 rev C.01.[9] Due to the asymmetry observed in the AC-TFTA crystal, two different trimers were considered, labeled as AC-TFTA-a and AC-TFTA-b. The modelling of the QM' region was carried out with the GFN2-xTB[10] Hamiltonian using the XTB software version 6.5.1.[11] In the embedding calculations the RESP charges were used at the CAM-B3LYP/6-311++G(d,p) and PBE-D3/6-31G(d) level of theory for the QM and QM' regions, respectively.

The energies of the Highest Occupied Crystalline and Lowest Unoccupied Crystalline Orbitals, HOCO and LUCO, respectively, were obtained from the periodic DFT calculations, as above mentioned and summarized in Table S1. For comparison, we included the energy of the Highest Occupied and Lowest Unoccupied Molecular Orbitals (HOMO and LUMO, respectively) computed as the isolated system (monomer, dyad or triad) in gas phase, and embedded in the point charges used in the ONIOM calculation at the CAM-B3LYP-D3/6-311++G(d,p) level of theory to simulate the crystalline environment. Figure S7 shows the relationship between the frontier MO's of the raw

components and the co-crystals. In both co-crystals, HOMO and LUMO are localised over the AC molecule and are slightly stabilised regarded to those in the pure AC crystal. AC-TFTA shows a degeneracy of HOMO and HOMO-1 (LUMO and LUMO+1) corresponding to each monomer of AC in the triad. While the LUMO+1 (LUMO+2) is related to the LUMO of PFBA (TFTA). Because of the level of localisation of the orbitals, the energies of the frontier orbitals are closer to the ones of AC. The computed DG_{HL} values correspond to the fundamental gap and as expected are overestimated with respect to the experimental fitting for the optical gap (Figure S6). The predicted optical gaps for the S_1-S_0 transitions are in better agreement with the calculations. We also performed a single point calculation with the B3LYP functional, which has been reported to accurately reproduce the HOMO-LUMO gap of organic chromophores. [S12] Nevertheless, such DFT approximation is well known for predicting spurious excited states at low energy, then we keep using CAM-B3LYP results for the analysis of photophysical properties of the co-crystals.

Geometry optimization in the S_1 energy surface was performed with the time dependent version of the CAM-B3LYP functional and the same basis set as specified above for the AC crystal but with the SVP basis set for the co-crystals, to decrease the computational cost. At the S_{1min} geometry, a single point calculation of each system was performed at the TD-CAM-B3LYP-D3/6-311++G(d,p), including the point charges of the embedded model.

To simulate the photoluminescence properties of the co-crystals, we predicted the minimum energy geometry in the S_1 potential energy surface by following the same ONIOM QM:QM' embbeded scheme as before. The emission energy of the pristine AC crystal is 2.99 eV (414 nm vs the experimental maximum determined at 507 nm). The shift of the co-crystals with respect to the raw component is negligible (less than 0.1 eV). SI includes de characterization of the emissive states, for both co-crystals PL happens from the S_{1min} geometry, which corresponds to the AC component with almost no influence of the acid molecule, explaining the very close emission of AC-PFBA and AC-TFTA with AC.

Differential Scanning Calorimetry (DSC) and Thermogravimetric Analysis (TGA)

DSC and TGA experiments were performed in a Netzsch STA 449 F3 Jupiter in a coupled/simultaneous mode. Samples were placed as powders in 5 mm Aluminum crucibles with a hole in the cap. The heating ramp employed was 10 °C per minute under nitrogen atmosphere.

Crystallographic information tables and X-Ray diffraction studies

X-Ray diffraction data were obtained at variable temperature from Bruker Smart APEX II CCD[S13] with graphite monochromatic MoKα radiation (λ=0.71073 Å) or CuKα radiation (1.54183 Å). Cell

refinement was carried out using SAINT V8.38A.[S14] Structure solution, final refinement and data output was carried out using SHELX-2014[S15] through direct methods. Non-hydrogen atoms were refined anisotropically and hydrogen atoms were placed in geometrically calculated positions using a riding model, with isotropic thermal parameters U_{iso}(H) = 1.2U_{eq}(C). Crystal structures were generated with Mercury 2022.3.0.[S16] Powder X-Ray diffraction data were collected at room temperature in a Bruker D8 Advance diffractometer, using CuKα radiation and Linxeye detector. It was operated at 30 kV and 25 mA with a Bragg-Brentano configuration in a 2θ interval of 5-50°, stepsize: 0.03°, steptime: 0.06 s.

Solid-state NMR Spectroscopy

Solid-state ^{13}C with CP MAS NMR spectra were obtained in a Bruker Avance II with a Larmor frequency of 500 MHz (11.7 T), equipped with a PH MAS DVT 500S1 BL3.2 N-P/F-H probe and Zirconia MAS rotors with VESPEL caps. The spectra were acquired by averaging between 1000 and 4000 transients, with a MAS rate of 20 kHz, delay time of 20 s, pulse width of 4 μs, and a contact time of 3 ms at 20 °C. Chemical shifts were referenced to adamantane (δ = 37.7 ppm). ^{19}F MAS were acquired in the same probe at a frequency of 470.6 MHz with rotation at 20 kHz, averaging scans, delay time of 10 s and pulse width of 4 μs. Chemical shifts were referenced externally to Teflon® (δ = -123.2 ppm) as secondary reference.

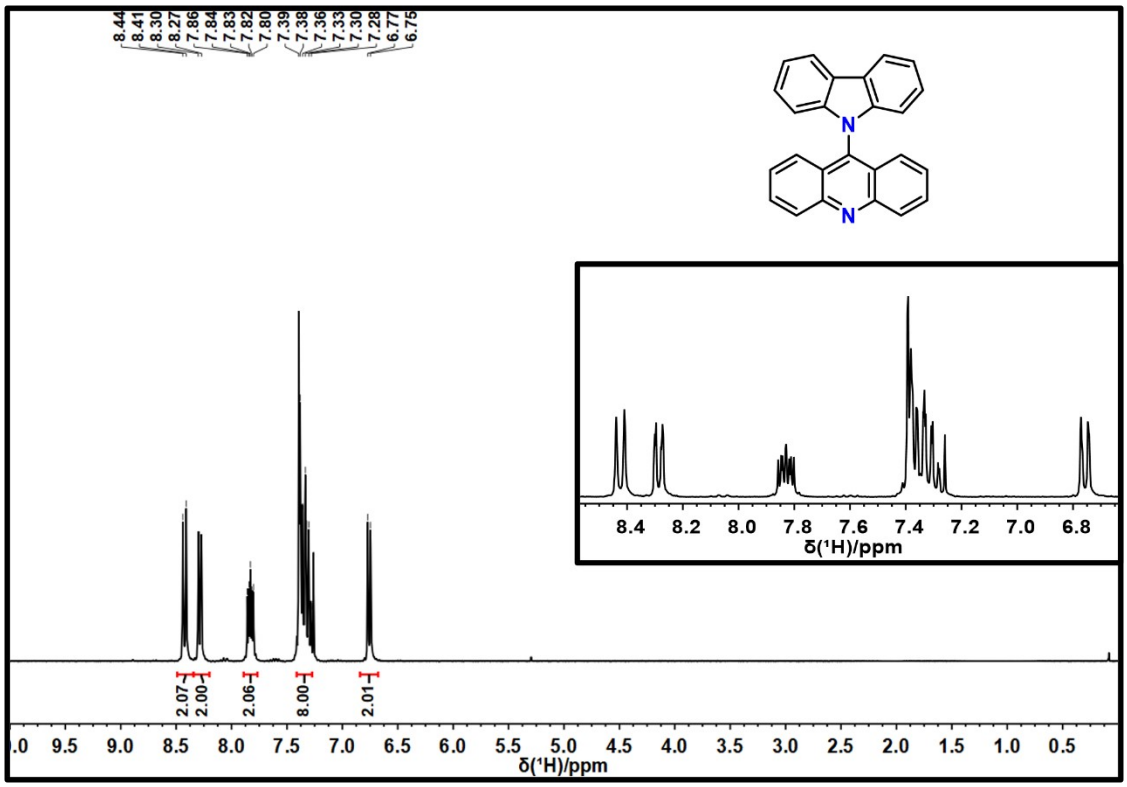

Figure S1. ^{1}H NMR spectra of compound **AC** ($CDCl_3$, 300 MHz, Room temperature).

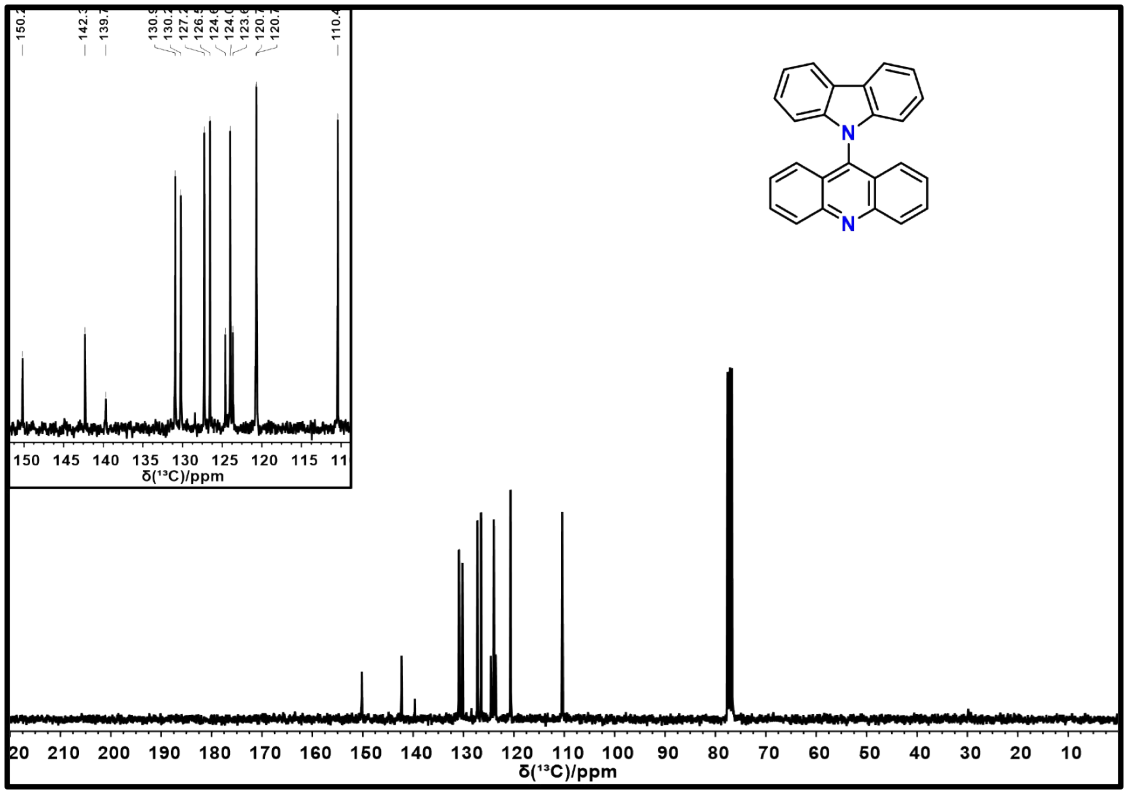

Figure S2. ^{13}C NMR spectra of compound **AC** ($CDCl_3$, 75 MHz, Room temperature).

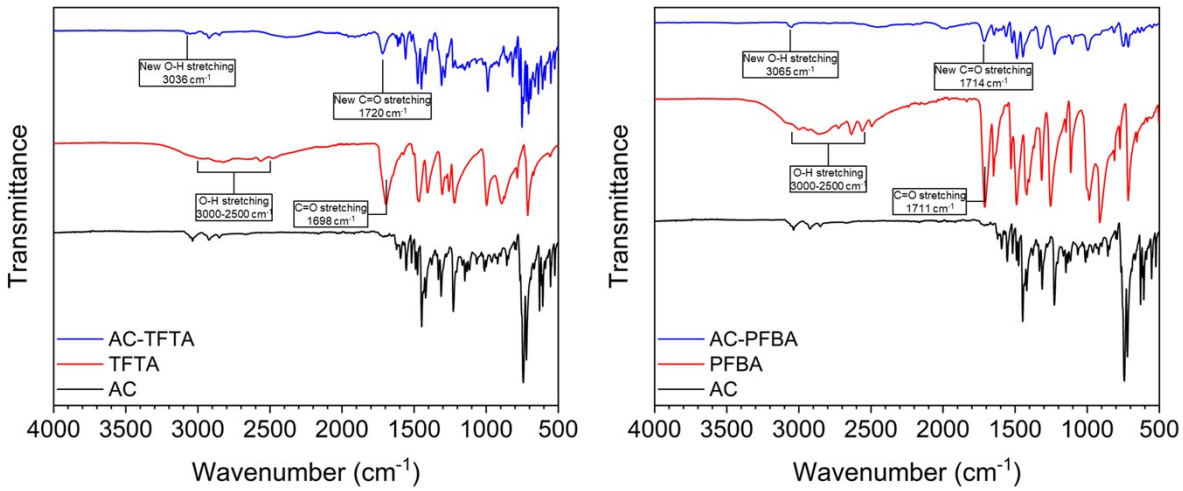

Figure S3. Comparative ATR-FTIR spectra of the starting materials AC, TFTA, PFBA and the cocrystals **AC-TFTA** and **AC-PFBA**.

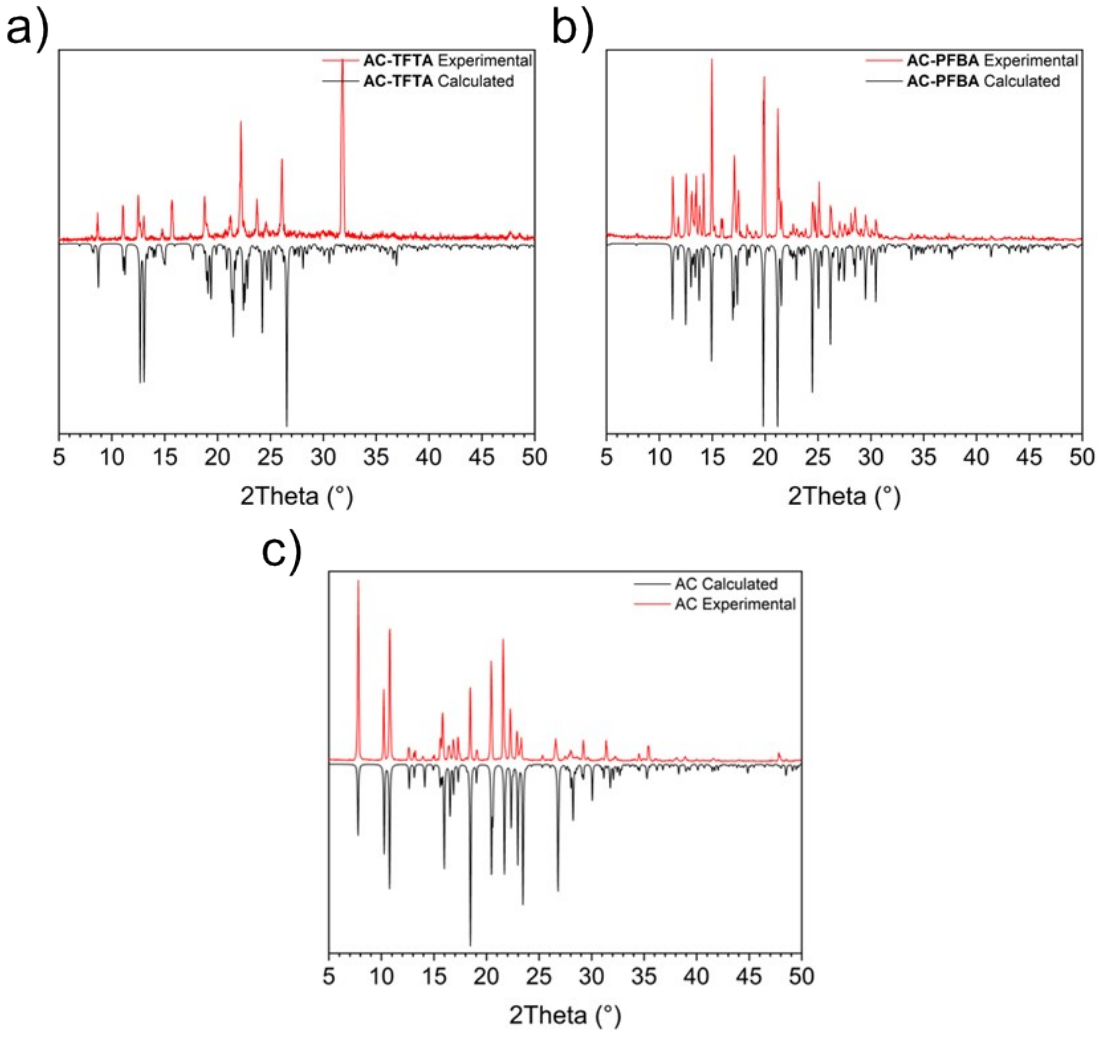

Figure S4. PXRD diffractograms of compound AC (solvent-free form).

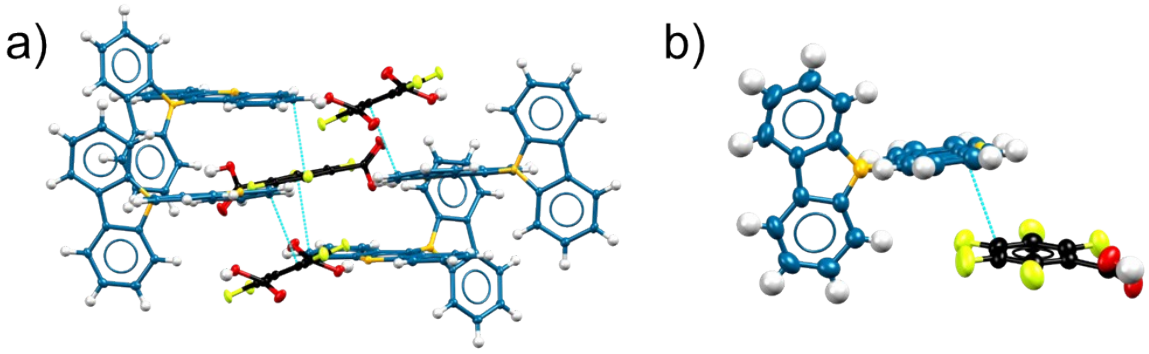

Figure S5. π-interactions between fragments in the crystalline packings of a) **AC-TFTA** and b) **AC-PFBA**, detrimental for fluorescence enhancement.

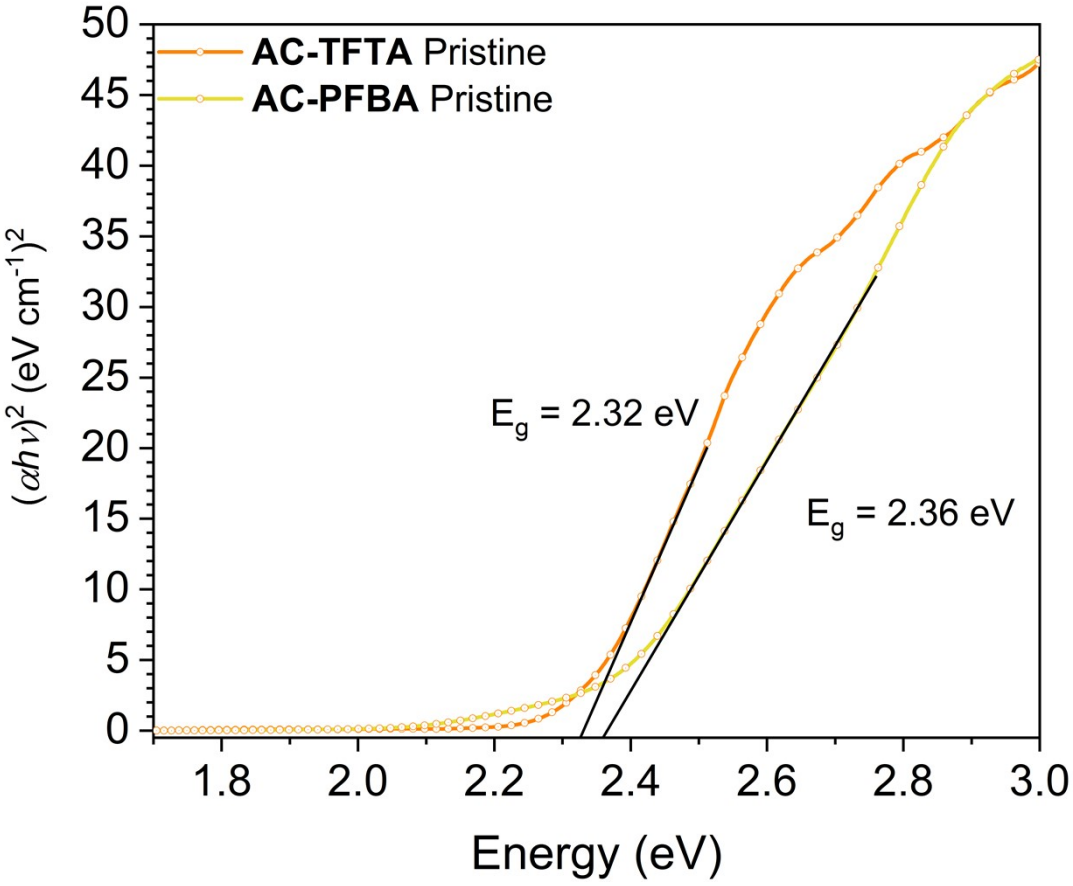

Figure S6. Tauc plots obtained from diffuse reflectance data with optical band gaps for pristine cocrystals.

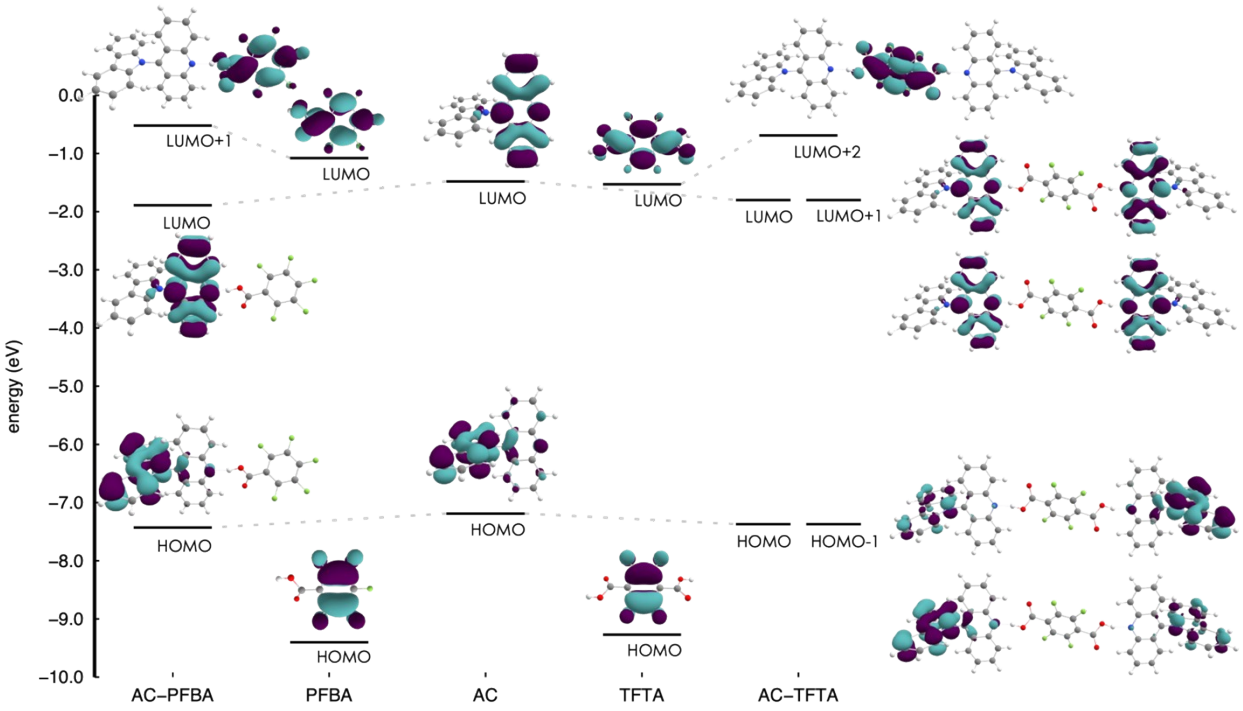

Figure S7. Frontier molecular orbitals diagram and representation of raw materials (AC, PFBA, TFTA) and co-crystals (AC-PFBA, AC-TFTA) computed at the CAM-B3LYP-D3/6-311++G(d,p) level of theory.

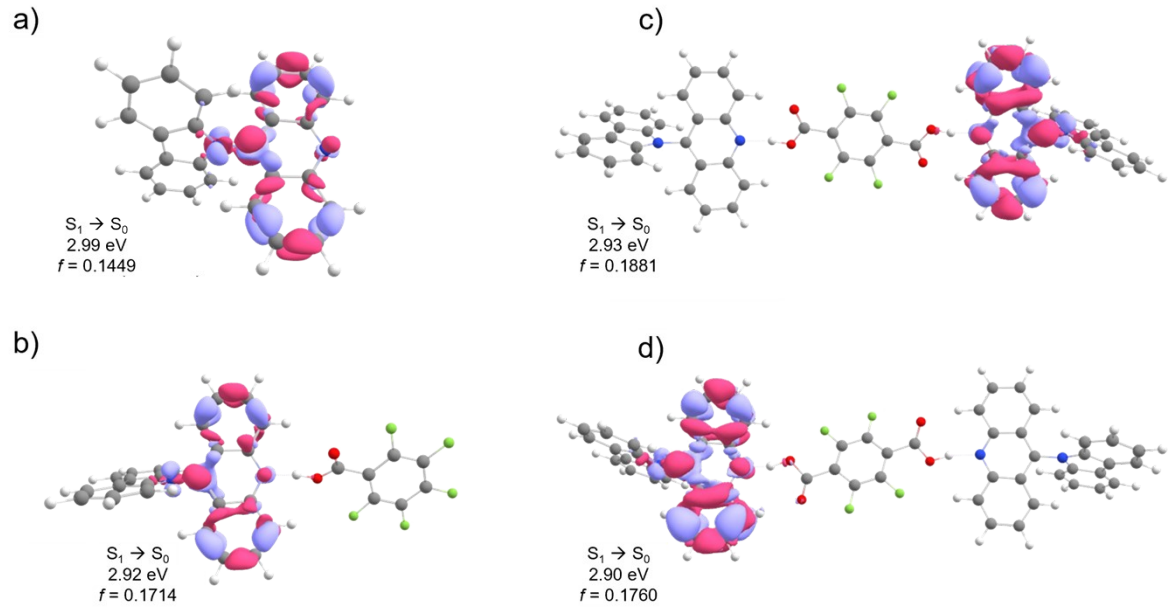

Figure S8. Characterization of the S_1 state of d) AC, e) AC-PFBA, f) AC-TFTA-a and, g) AC-TFTA-b. Electronic density difference plots (pink positive, blue negative) for the $S_0 \rightarrow S_1$ transition computed at TD-CAM-B3LYP-D3/6-311++G(d,p) level of theory. Excitation energies are reported in eV and the oscillator strength presented in parentheses. Isosurface contour value = 0.02 for d) and e) and 0.01 for f) and g).

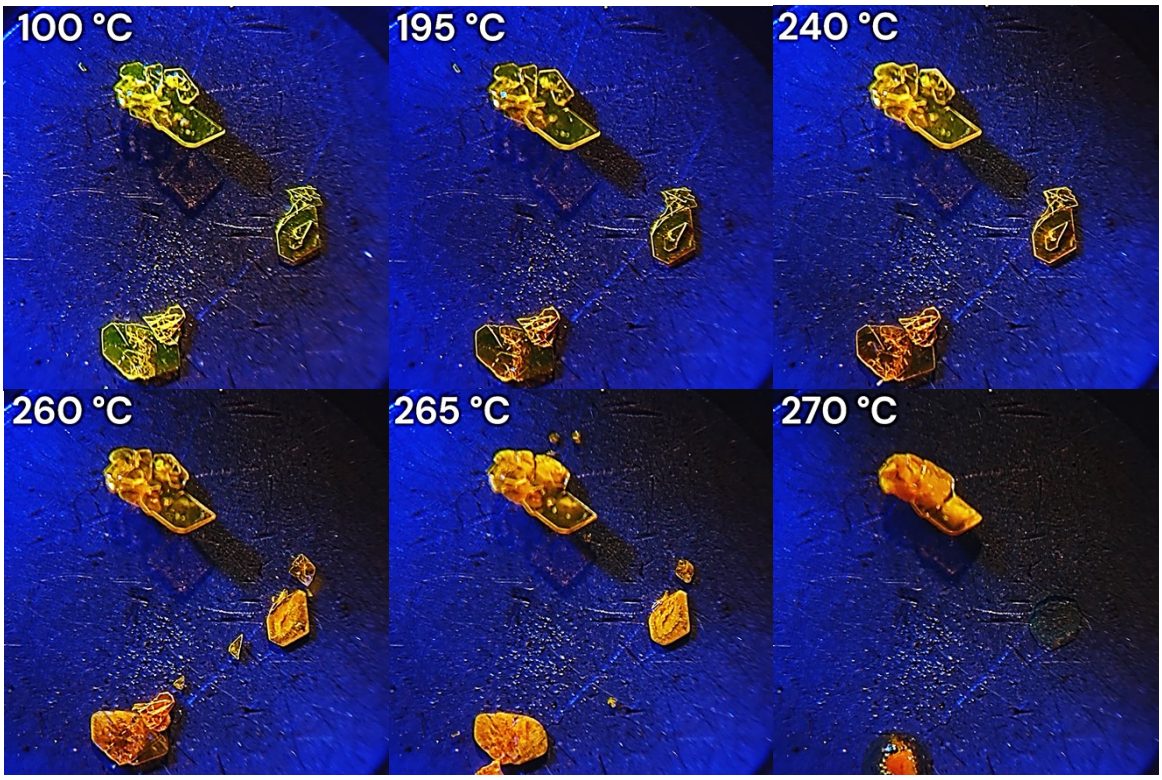

Figure S9. Photographs of **AC-TFTA** single crystals on the hot plate of a Fisher-Johns apparatus, displaying jumping due to heating.

a)

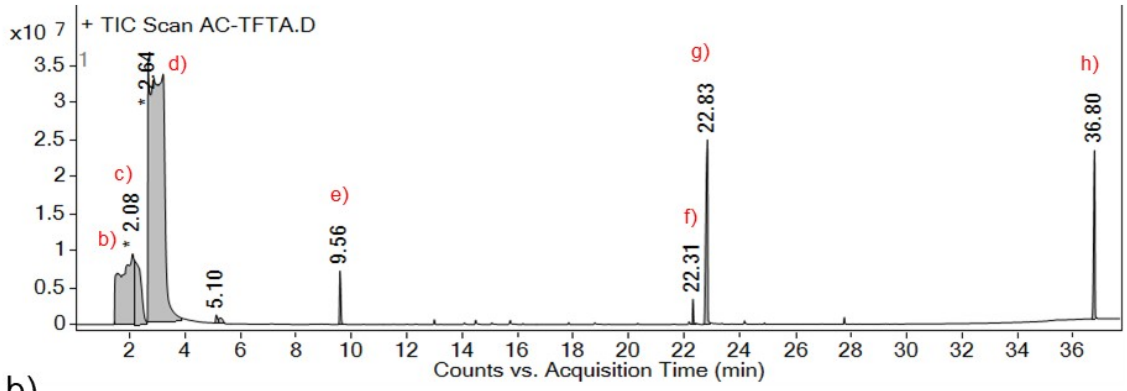
+ TIC Scan AC-TFTA.D
x10 7
b)
c)
d)
e)
f)
g)
h)
2.08
2.64
5.10
9.56
22.31
22.83
36.80
Counts vs. Acquisition Time (min)

b)

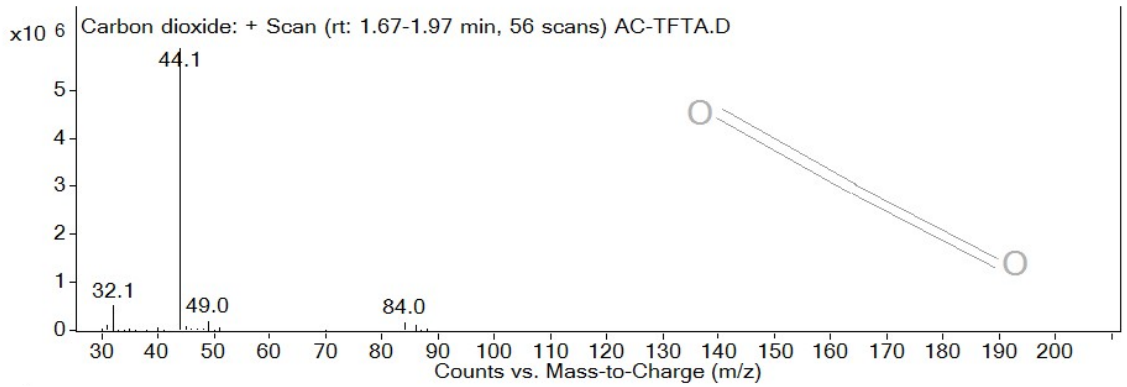
Carbon dioxide: + Scan (rt: 1.67-1.97 min, 56 scans) AC-TFTA.D
x10 6
44.1
32.1
49.0
84.0
O
O
Counts vs. Mass-to-Charge (m/z)

c)

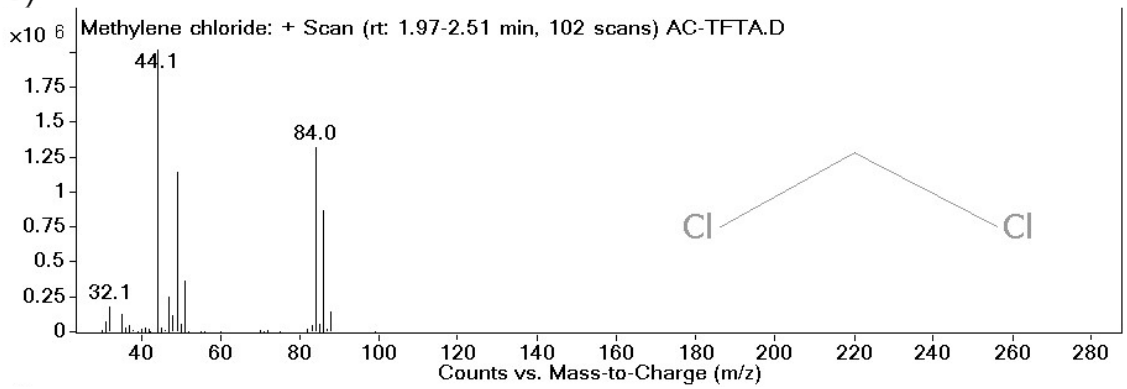
Methylene chloride: + Scan (rt: 1.97-2.51 min, 102 scans) AC-TFTA.D
x10 6
44.1
84.0
32.1
Cl
Cl
Counts vs. Mass-to-Charge (m/z)

d)

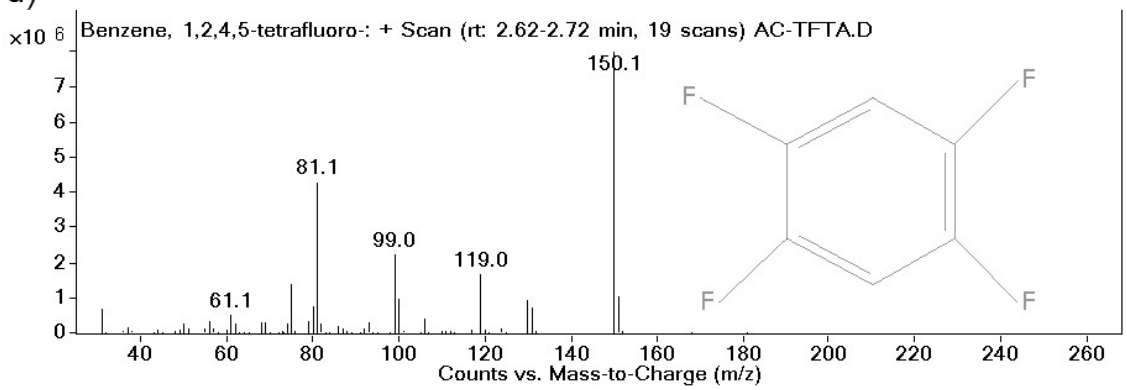
Benzene, 1,2,4,5-tetrafluoro-: + Scan (rt: 2.62-2.72 min, 19 scans) AC-TFTA.D
x10 6
150.1
81.1
99.0
119.0
61.1
F
F
F
F
Counts vs. Mass-to-Charge (m/z)

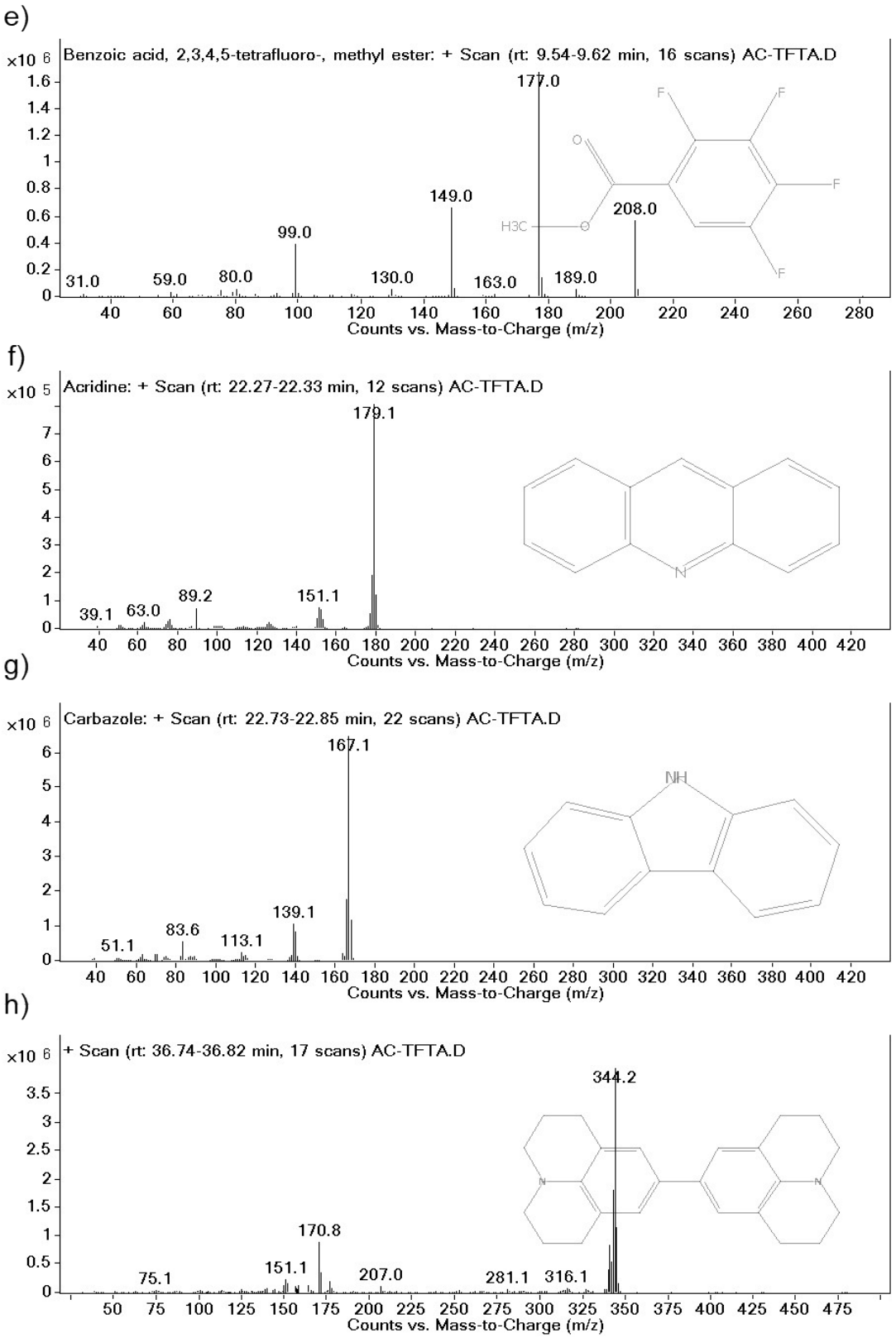

Figure S10. a) Gas chromatogram of the volatile mixture injected after the heating of pristine **AC-TFTA**; b-h) Compounds found in the mixture associated with their respective mass spectrogram and the corresponding retention time.

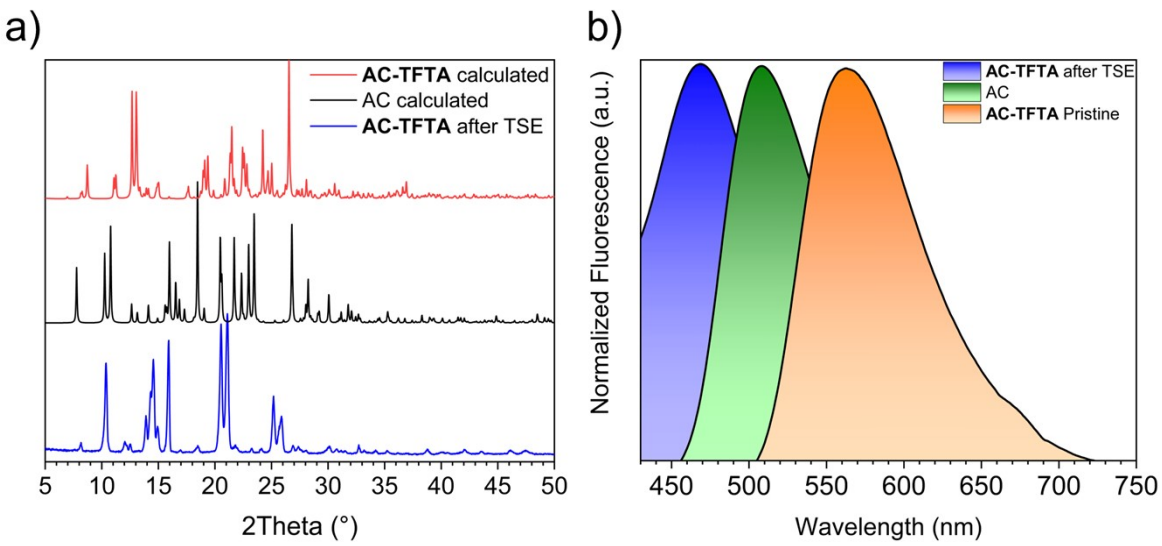

Figure S11. Characterization of residual powder after heating and thermosalient effect of **AC-TFTA**: a) comparative PXRD diffractogram and b) comparative solid-state fluorescence spectra, both against the pristine AC and **AC-TFTA** pristine.

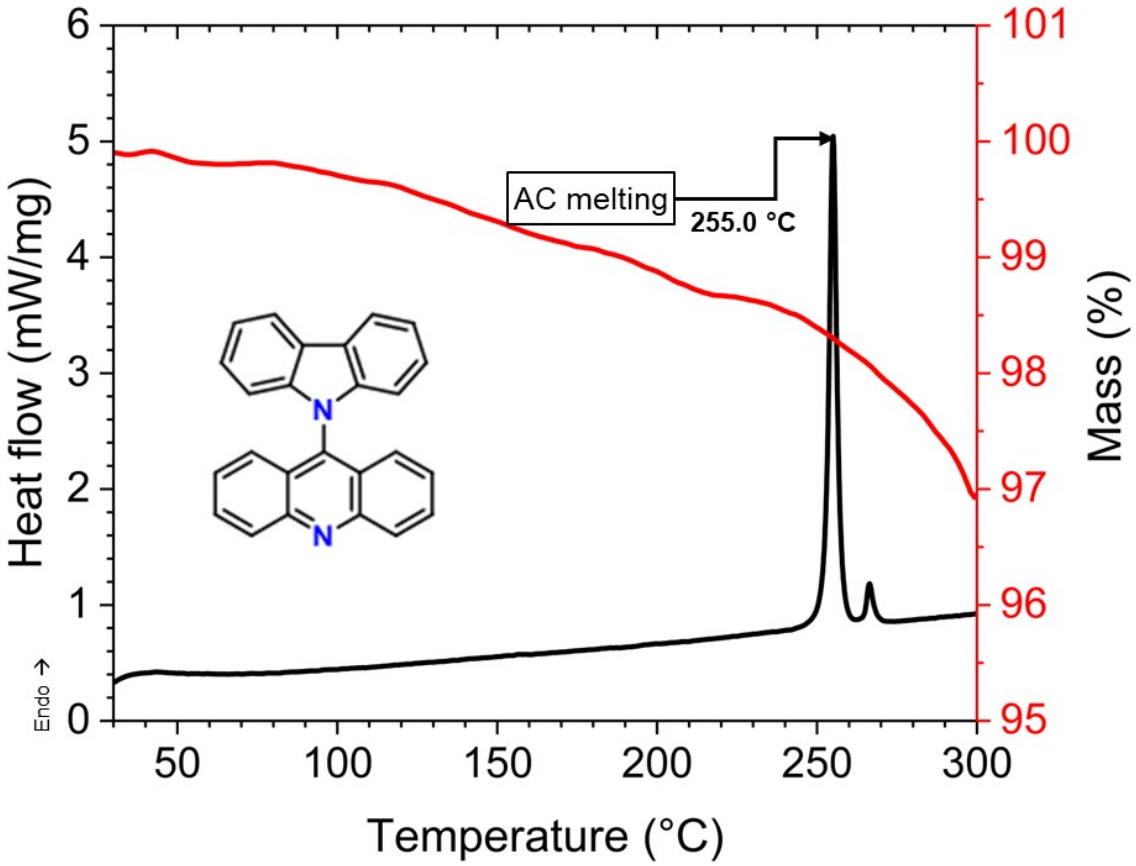

Figure S12. DSC and TGA profiles of AC as solvent-free form.

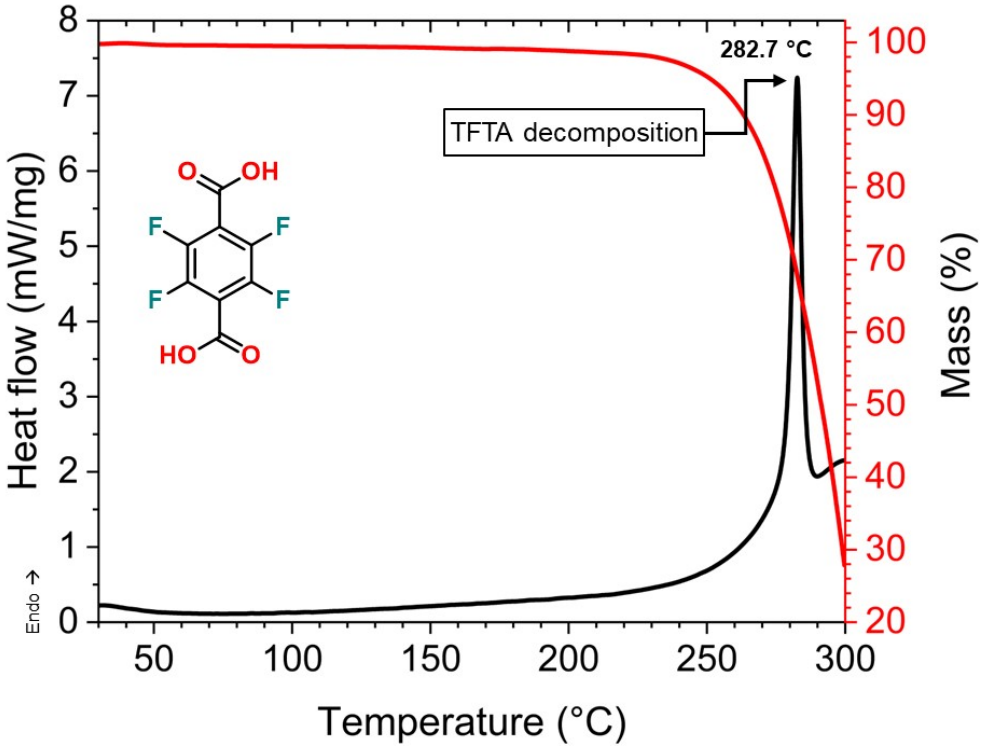

Figure S13. DSC and TGA profiles of TFTA.

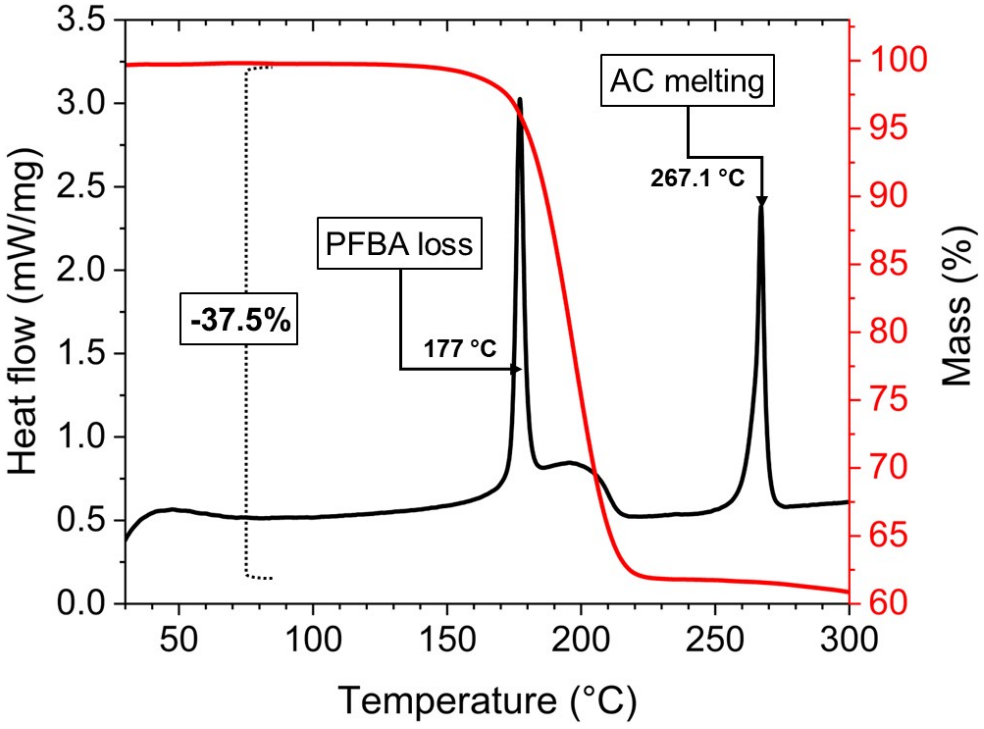

Figure S14. DSC and TGA profiles of pristine **AC-PFBA**.

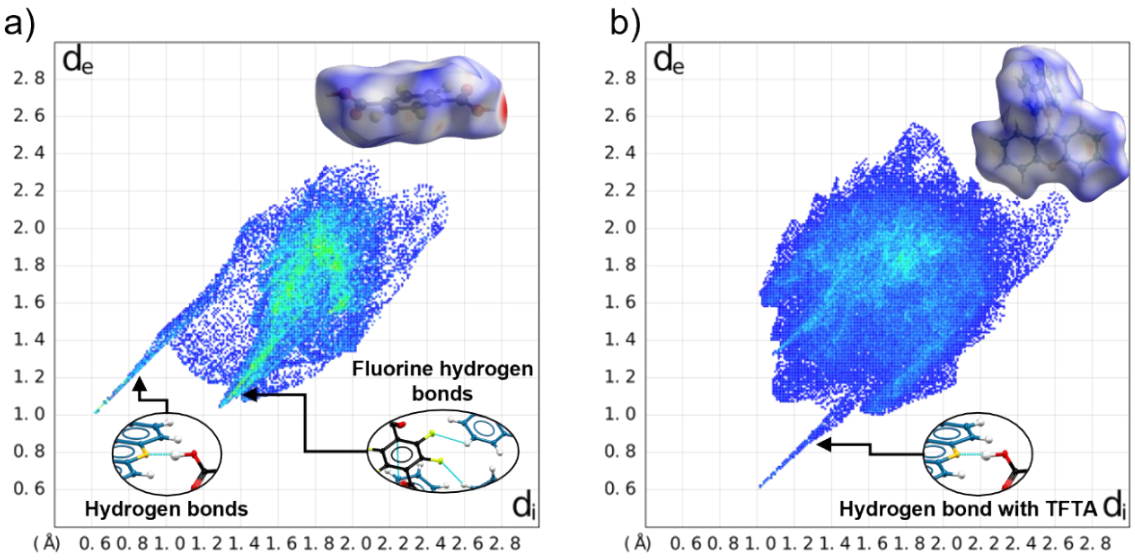

Figure S15. Fingerprint plots of each coformer in the **AC-TFTA** cocrystal with insets of the most important interactions: a) TFTA and b) AC.

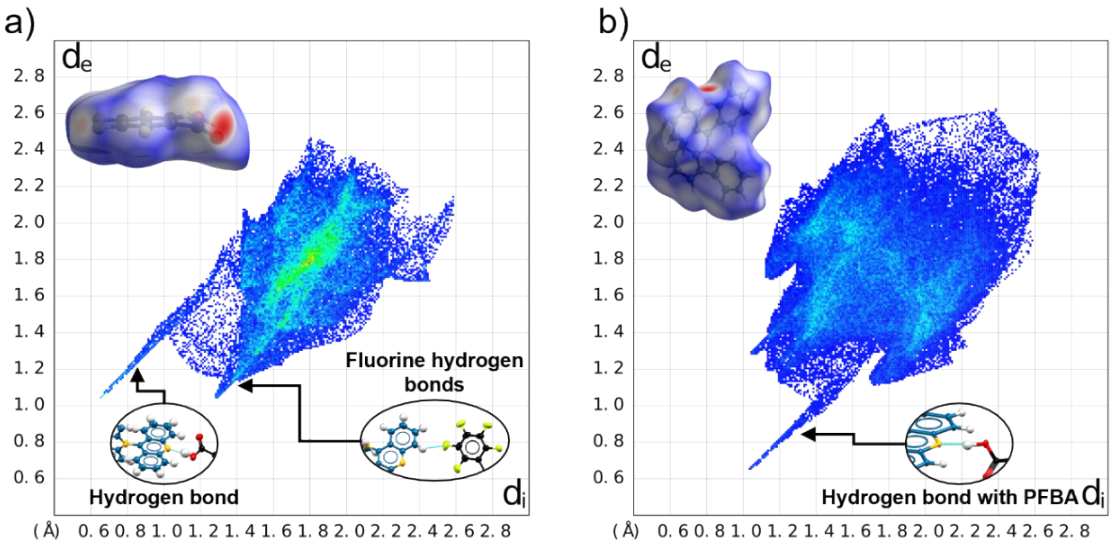

Figure S16. Fingerprint plots of each coformer in the **AC-PFBA** cocrystal with insets of the most important interactions: a) PFBA and b) AC.

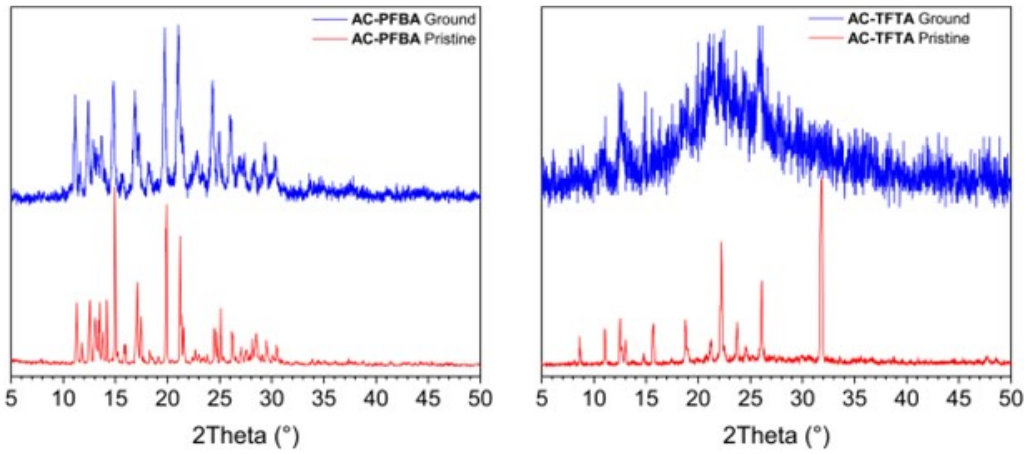

Figure S17. Powder X-Ray diffractograms obtained from ground cocrystals (850 rpm, 60 minutes, 5 mm Zirconium oxide grinding balls).

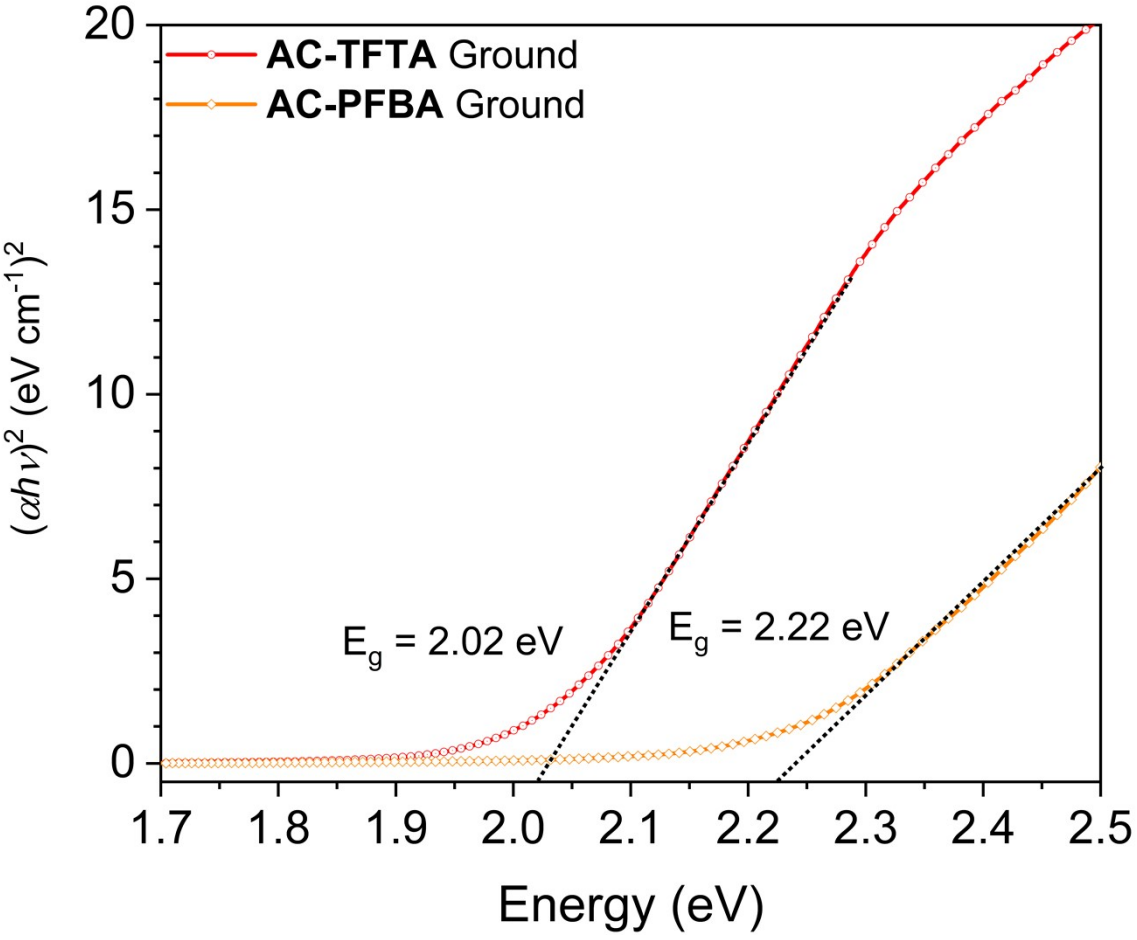

Figure S18. Tauc plots obtained from diffuse reflectance data with optical band gaps for ground powders of cocrystals.

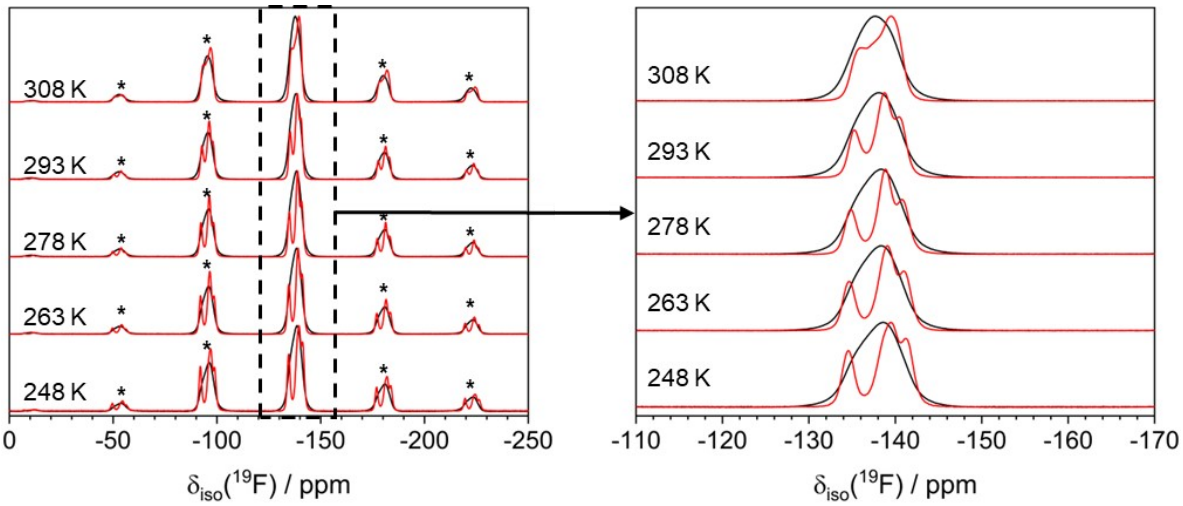

Figure S19. ^{19}F MAS spectra (470.6 MHz, Spin Rate = 20 kHz, d_1 = 10 s) of cocrystal **AC-TFTA** at several temperatures and zoomed region between -110 and -170 ppm (right). Red line depicts the spectra of pristine sample and black represents the spectra of ground cocrystal. Sets of signals marked with '*' are referred to spinning sidebands.

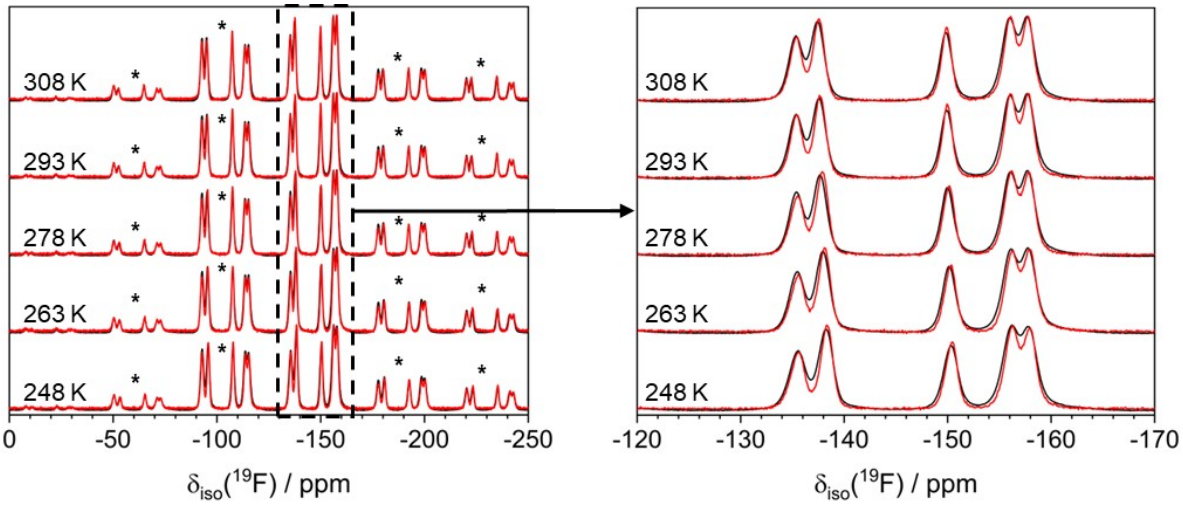

Figure S20. ^{19}F MAS spectra of cocrystal **AC-PFBA** (470.6 MHz, Spin Rate = 20 kHz, d_1 = 10 s) at several temperatures and zoomed region between -120 and -170 ppm (right). Red line depicts the spectra of pristine sample and black represents the spectra of ground cocrystal. Sets of signals marked with '*' are referred to spinning sidebands.

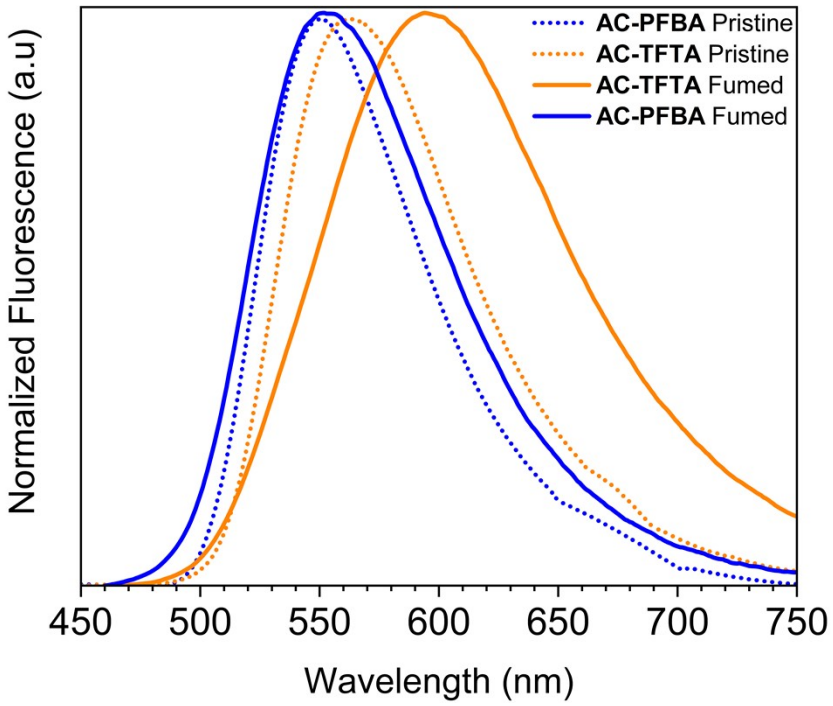

Figure S21. Solid-state fluorescence spectra of fumed solids. The spectra associated with the fumed solids is displayed as continuous lines and the comparison against the pristine samples is dotted.

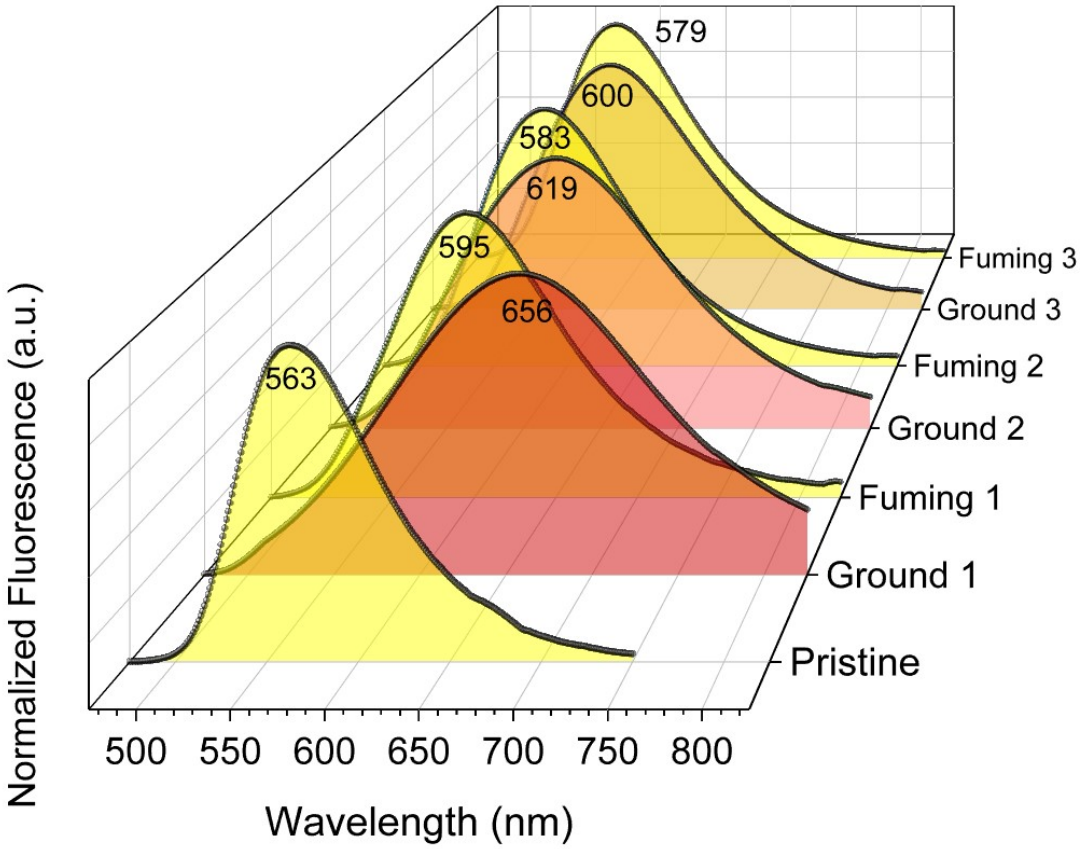

Figure S22. Progressive solid-state fluorescence spectra obtained from the fatigue tests on **AC-TFTA**.

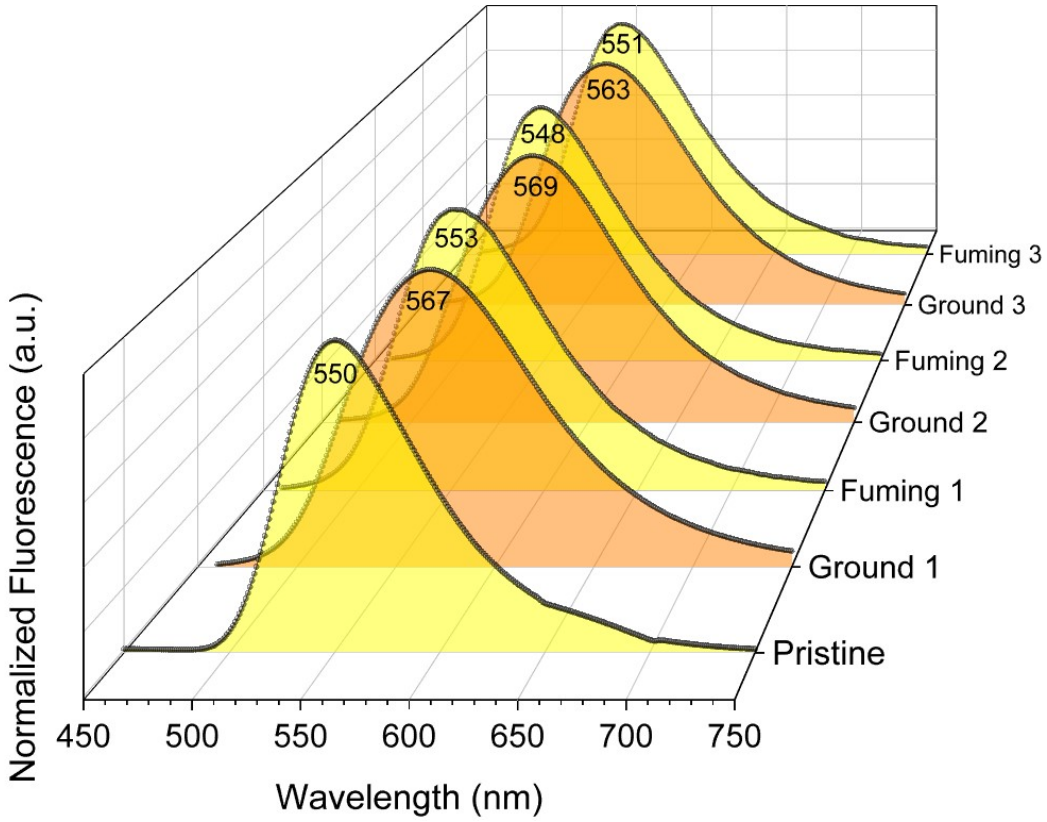

Figure S23. Progressive solid-state fluorescence spectra obtained from the fatigue tests on **AC-PFBA**.

Table S1. Absolute energy of frontier crystalline and molecular orbitals of co-crystals and their components. Highest Occupied and Lowest Unoccupied Crystalline Orbital (HOCO an LUCO) are computed with PBE-D3. Highest Occupied and Lowest Unoccupied Molecular Orbitals (HOMO and LUMO) are computed at the CAM-B3LYP-D3/6-311++G(d,p) level of theory. Values in parenthesis were computed at B3LYP-D3/6-311++G(d,p). Energies are reported in eV.

	periodic model			isolated system			embedded model		
	HOCO	LUCO	DG_{HL}	HOMO	LUMO	DG_{HL}	HOMO	LUMO	DG_{HL}
AC	0.25	1.95	1.70	-7.19	-1.48	5.71	-7.01	-1.20	5.81
							(-5.72)	(-2.29)	(3.43)
PFBA	-0.54	2.74	3.28	-9.40	-1.08	8.32			
TFTA	0.13	2.81	2.68	-9.27	-1.53	7.74			
AC-PFBA	-0.08	1.64	1.72	-7.43	-1.89	5.54	-7.61	-1.84	5.77
							(-6.30)	(-2.93)	(3.37)
AC-TFTA	-0.08	1.84	1.92	-7.37	-1.80	5.57	-7.11.	-1.28	5.83
							(-5.82)	(-2.38)	(3.44)

Table S2. Vertical excitation energy (ee) in eV, oscillator strength (f) and character of the lowest-lying excited singlets of AC, AC-PFBA and AC-TFTA at the ground state geometry computed at the B3LYP-D3/6-311++G(d,p) level of theory. iCT = intraCharge Transfer, CT = Charge Transfer, LE = Local Excitation.

	AC		AC-PFBA			AC-TFTA		
state	ee	f	ee	f	character	ee	f	character
S_1	2.76	0.0114	2.71	0.0148	iCT (AC)	2.78	0.0176	iCT (AC) +CT (AC→AC)
S_2	3.18	0.0003	3.14	0.0303	iCT (AC)	2.78	0.0071	iCT (AC) +CT (AC→AC)
S_3	3.22	0.0822	3.14	0.0689	LE (AC)	3.12	0.2064	CT (AC→AC) + iCT (AC)
S_4	3.83	0.0063	3.85	0.0664	LE (AC)	3.13	0.0002	CT (AC→AC) + iCT (AC)
S_5	3.89	0.0435	3.95	0.0000	CT (PFBA→AC)	3.18	0.0013	CT (AC→AC) + iCT (AC)
S_6	4.00	0.0358	4.01	0.0049	LE (AC)	3.18	0.0011	CT (AC→AC) + iCT (AC)
S_7	4.10	0.0009	4.03	0.0407	LE (AC) + CT (AC→PFBA)	3.29	0.0000	CT (AC→AC) + iCT (AC)
S_8	4.34	0.0039	4.11	0.0003	CT (PFBA→AC)	3.29	0.0000	CT (AC→AC) + iCT (AC)
S_9	4.37	0.0101	4.19	0.0000	CT (PFBA→AC)	3.41	0.0000	CT (AC→AC) + iCT (AC)
S_{10}	4.38	0.0151	4.28	0.0003	LE (AC)	3.41	0.0000	CT (AC→AC) + iCT (AC)

Table S3. Final refinement parameters for structures AC as solvated forms.

Identification code	**AC-Toluene_solvate_100K**		**AC-THF_solvate_100K**	
Empirical formula	$C_{23}H_{24}N_2$		$C_{29}H_{24}N_2O$	
Formula weight	436.53		416.50	
Temperature [K]	100(2)		100(2)	
Wavelength [Å]	0.71073		0.71073	
Crystal system	Monoclinic		Monoclinic	
Space group	C2/c		C2/c	
Unit cell dimensions	a = 13.8355(8) Å	a= 90°	a = 14.1494(3) Å	a= 90°
	b = 10.5769(6) Å	b= 112.5690(10)°	b = 10.4352(2) Å	b= 96.6880(10)°
	c = 17.1587(13) Å	g = 90°	c = 15.0991(4) Å	g = 90°
Volume [Å^3]	2318.7(3)		2214.24(9)	
Z	4		4	
Density (calculated) [g cm^{-3}]	1.251		1.249	
Absorption coefficient [mm^{-1}]	0.073		0.076	
F(000)	923		880	
Crystal size [mm]	0.420 x 0.392 x 0.364		0.288 x 0.157 x 0.076	
Theta range for data collection [°]	2.500 to 30.507		2.431 to 32.592°	
Index ranges	$-17 \le h \le 19$ $-15 \le k \le 15$ $-24 \le l \le 24$		$-21 \le h \le 21$ $-15 \le k \le 15$ $-22 \le l \le 22$	
Reflections collected	13471		32008	
Independent reflections	3540 [R(int) = 0.0330]		4042 [R(int) = 0.0337]	
Completeness to theta = 25.242°	99.80%		99.7%	
Absorption correction	Semi-empirical from equivalents		Semi-empirical from equivalents	
Max. and min. transmission	0.7464 and 0.66770		0.7464 and 0.6999	
Refinement method	Full-matrix least-squares on F^2		Full-matrix least-squares on F^2	
Data / restraints / parameters	3540 / 0 / 188		4042 / 0 / 178	
Goodness-of-fit on F^2	1.048		1.082	
Final R indices [I>2sigma(I)]	R1 = 0.0470 wR2 = 0.1237		R1 = 0.0584 wR2 = 0.1758	
R indices (all data)	R1 = 0.0578 wR2 = 0.1327		R1 = 0.0695 wR2 = 0.1870	
Extinction coefficient	n/a		n/a	
Largest diff. peak and hole [eÅ^{-3}]	0.392 and -0.224		0.575 and -0.296	
CCDC Number	2351862		2351863	

Table S4. Final refinement parameters for cocrystals.

Identification code	**AC-TFTA_100K**		**AC-PFBA_300K**	
Empirical formula	$C_{58}H_{34}F_4N_4O_4$		$C_{32}H_{17}F_5N_2O_2$	
Formula weight	926.89		556.47	
Temperature [K]	100(2)		298(2)	
Wavelength [Å]	0.71073		1.54178	
Crystal system	Triclinic		Monoclinic	
Space group	P-1		$P2_1/c$	
Unit cell dimensions	a = 8.2289(4) Å	a= 90.7200(10)°	a = 22.6117(3) Å	a= 90°
	b = 12.7093(7) Å	b= 95.6660(10)°	b = 8.39190(10) Å	b= 92.8810(10)°
	c = 20.6345(10) Å	g = 91.6730(10)°	c = 13.2304(2) Å	g = 90°
Volume [$Å^3$]	2118.23(19)		2507.36(6)	
Z	2		4	
Density (calculated) [g cm^{-3}]	1.453		1.474	
Absorption coefficient [mm^{-1}]	0.104		1.010	
F(000)	956		1136	
Crystal size [mm]	0.386 x 0.214 x 0.207		0.402 x 0.398 x 0.388	
Theta range for data collection [°]	2.010 to 31.506		3.915 to 70.054	
Index ranges	$-12 \le h \le 12$ $-18 \le k \le 18$ $-29 \le l \le 29$		$-27 \le h \le 26$ $-10 \le k \le 10$ $-16 \le l \le 16$	
Reflections collected	51935		40172	
Independent reflections	14071 [R(int) = 0.0358]		4711 [R(int) = 0.0342]	
Completeness to theta = 25.242°	99.9%		99.0%	
Absorption correction	Semi-empirical from equivalents		Semi-empirical from equivalents	
Max. and min. transmission	0.7464 and 0.6843		0.7535 and 0.6209	
Refinement method	Full-matrix least-squares on F^2		Full-matrix least-squares on F^2	
Data / restraints / parameters	14071 / 0 / 637		4711 / 270 / 393	
Goodness-of-fit on F^2	1.028		1.042	
Final R indices [I>2sigma(I)]	R1 = 0.0426 wR2 = 0.1088		R1 = 0.0376 wR2 = 0.1020	
R indices (all data)	R1 = 0.0562 wR2 = 0.1177		R1 = 0.0392 wR2 = 0.1037	
Extinction coefficient	n/a		0.0042(3)	
Largest diff. peak and hole [e$Å^{-3}$]	0.537 and -0.270		0.202 and -0.207	
CCDC Number	2351864		2351865	

References

[S1] S. Zeghada, G. Bentabed-Ababsa, O. Mongin, W. Erb, L. Picot, V. Thiéry, T. Roisnel, V. Dorcet, F. Mongin, *Tetrahedron*, 2020, **76**, 131435.

[S2] Mackenzie, C. F.; Spackman, P. R.; Jayatilaka, D.; Spackman, M. A. *IUCrJ* **2017**, *4*, 575–587.

[S3] Bucko, T., Hafner, J., Lebègue, S., Angyán, J. G. (2010). Improved description of the structure of molecular and layered crystals: ab initio DFT calculations with van der Waals corrections. *J. Phys. Chem.* A, **2010**, 114, 11814-11824.

[S4] G. Kresse and J. Hafner, Phys. Rev. B 47, 558 (1993); ibid 49, 14 251 (1994).

[S5] M. Rivera, M. Dommett, R. Crespo-Otero. ONIOM (QM: QM′) electrostatic embedding schemes for photochemistry in molecular crystals. J. Chem. Theory Comput., 2019, 15, 4,2504-2516.

[S6] M. Rivera, M. Dommett, A. Sidat, W. Rahim, and R. Crespo-Otero. fromage: A library for the study of molecular crystal excited states at the aggregate scale. J. Comput. Chem., 2020, 41, 1045-1058.

[S7] Yanai, Takeshi, David P. Tew, and Nicholas C. Handy. "A new hybrid exchange–correlation functional using the Coulomb-attenuating method (CAM-B3LYP)." Chemical physics letters 393.1-3 (2004): 51-57.

[S8] S. Grimme, J. Antony, S. Ehrlich, and H. Krieg, "A consistent and accurate ab initio parametrization of density functional dispersion correction (DFT-D) for the 94 elements H-Pu," J. Chem. Phys. 132, 154104 (2010).

[S9] M. J. Frisch, G. W. Trucks, H. B. Schlegel, G. E. Scuseria, M. A. Robb, J. R. Cheeseman, G. Scalmani, V. Barone, G. A. Petersson, H. Nakatsuji, X. Li, M. Caricato, A. V. Marenich, J. Bloino, B. G. Janesko, R. Gomperts, B. Mennucci, H. P. Hratchian, J. V. Ortiz, A. F. Izmaylov, J. L. Sonnenberg, D. Williams-Young, F. Ding, F. Lipparini, F. Egidi, J. Goings, B. Peng, A. Petrone, T. Henderson, D. Ranasinghe, V. G. Zakrzewski, J. Gao, N. Rega, G. Zheng, W. Liang, M. Hada, M. Ehara, K. Toyota, R. Fukuda, J. Hasegawa, M. Ishida, T. Nakajima, Y. Honda, O. Kitao, H. Nakai, T. Vreven, K. Throssell, J. A. Montgomery, Jr., J. E. Peralta, F. Ogliaro, M. J. Bearpark, J. J. Heyd, E. N. Brothers, K. N. Kudin, V. N. Staroverov, T. A. Keith, R. Kobayashi, J. Normand, K. Raghavachari, A. P. Rendell, J. C. Burant, S. S. Iyengar, J. Tomasi, M. Cossi, J. M. Millam, M. Klene, C. Adamo, R. Cammi, J. W. Ochterski, R. L. Martin, K. Morokuma, O. Farkas, J. B. Foresman, and D. J. Fox, Gaussian, Inc., Wallingford CT, 2019.

[S10] C. Bannwarth, S. Ehlert and S. Grimme., J. Chem. Theory Comput., 2019, 15, 1652-1671.

[S11] C. Bannwarth, E. Caldeweyher, S. Ehlert, A. Hansen, P. Pracht, J. Seibert, S. Spicher, S. Grimme, WIREs Comput. Mol. Sci., 2020, 11, e01493.

[S12] Ong, Bee Kian, Kai Lin Woon, and Azhar Ariffin. "Evaluation of various density functionals for predicting the electrophosphorescent host HOMO, LUMO and triplet energies." Synthetic metals 195 (2014): 54-60.

[S13] APEX2 Version 2008.3-0/2.2-0, Bruker AXS, Inc., Madison, WI, 2007.

[S14] Bruker. (2006b). SAINT, Version 8.38 (Bruker AXS Inc.).

[S15] G. M. Sheldrick, *Acta Cryst. A.*, 2008, **64**, 112–122.

[S16] C. F. Macrae, I. Sovago, S. J. Cottrell, P. T. A. Galek, P. McCabe, E. Pidcock, M. Platings, G. P. Shields, J. S. Stevens, M. Towler and P. A. Wood, *J. Appl. Cryst.*, 2020, **53**, 226-235.